UNIVERSITY OF CALIFORNIA,
IRVINE

The Development of Real-Time Insulin and Calcium Optical Biosensors using Förster Resonance Energy Transfer

THESIS

Submitted in partial satisfaction of the requirements
for the degree of

MASTER OF SCIENCE

in Chemistry

by

Jessica Ngoc-Han Pham

Thesis Committee:
Professor Gregory A. Weiss, Chair
Professor Jennifer A. Prescher
Professor David Van Vranken

2020

TABLE OF CONTENTS

LIST OF FIGURES

LIST OF TABLES

ACKNOWLEDGEMENTS

I would like to express an appreciation to my committee chair, Professor Gregory A. Weiss, who has shown strong support and guidance, especially through a stressful pandemic. He continually expressed excitement and innovation in regard to the science that inspires me and others in the field.

I would like to thank my committee members, Professor Jennifer A. Prescher and Professor David Van Vranken, whose work and expertise demonstrated the importance of creativity in science.

I would like to acknowledge the organizations that provided the financial support that allows the opportunity to work on a worthwhile project, the Juvenile Diabetes Research Foundation (JDRF) and the Leona M. and Harry B. Helmsley Charitable Trust.

ABSTRACT OF THE THESIS

The Development of Real-Time Insulin and Calcium Optical Biosensors using Förster Resonance Energy Transfer

by

Jessica Ngoc-Han Pham

Master of Science in Chemistry

University of California, Irvine, 2020

Professor Gregory A. Weiss, Chair

Optical FRET biosensors allow for real-time biomarker detection for healthcare applications. In this thesis, I discuss the development of real-time FRET sensors for insulin (Project I) and calcium (Project II) for applications in diabetes management and improved clinical practices, respectively. Both biosensors are based on the structures of native proteins that interact specifically with either insulin or calcium in real-time and undergo conformational changes. These conformational changes are harnessed with fluorescent proteins and small molecules to generate a FRET response. For the insulin biosensor (Project I), the sensor is modelled on insulin binding domains for the human insulin receptor (InR), whereas the calcium sensor is developed from an existing troponin C-based FRET biosensor, Twitch-2B. Using a combination of rational design, high diversity random mutagenesis phage display libraries and a high-throughput FRET screening platform, libraries of InR variants are screened to identify a potential insulin sensor with specific dose-dependent insulin binding and FRET response. Project II involves the optimization of the Twitch-2B FRET calcium sensor for integration in implantable devices. Towards this goal, we develop a FRET construct using SNAP- and CLIP-tags that can be stably expressed and is not prone to photobleaching.

INTRODUCTION

Biosensors integrate technologies from biology, chemistry, and engineering for the detection of biomarkers associated with diseases such as cancer, kidney disease, and diabetes.[1] Optical biosensors offer the advantage of providing a direct means of detection and allowing the tunability for high sensitivity and specificity.[2] Specifically, Förster Resonance Energy Transfer (FRET) can detect conformational changes that certain proteins undergo upon ligand binding. In these instances, having fluorophore-linked proteins allows radiation-free energy transfer between the fluorophores in close proximity to each other (i.e. within 10 nm).[3] This opens the door to many healthcare applications, including real-time monitoring of metabolite levels, diagnosing biomarker-related diseases, and determining drug effectiveness.[1] Our goal is to develop a real-time optical FRET sensor for insulin and calcium detection.

Project I: Real-time insulin sensor for T1D management

In 2017, the Centers for Disease Control and Prevention reported that approximately 30.3 million people in the U.S. suffer from diabetes.[4] Individuals afflicted with the disease have a shortened lifespan and live with constant awareness of its many risks, such as stroke, limb amputation, retinopathy-induced blindness, kidney dysfunction, unconsciousness, and if left untreated, death.[5,6] Individuals with type 1 diabetes (T1D) cannot produce insulin due to loss of the hormone-producing cell cluster, termed islet cells, in the pancreas. Constant monitoring of the individuals' glucose levels and administration of insulin is essential. Current technology is moving towards automation of these processes through an artificial pancreas.

For glucose control in T1D individuals, the artificial pancreas consists of a continuous glucose monitor (CGM), which measures and transmits interstitial glucose levels to the insulin pump. The latter then delivers an appropriate insulin dosage based on the CGM data.[6] However, the artificial pancreas estimates the amount of insulin on-board (IOB), or insulin active in the body, based solely on glucose levels. Several factors can change the rate at which insulin depletes, such as physical activity or consumption of a meal. Additionally, lack of blood circulation can cause insulin to accumulate within the interstitial fluid and enter circulation irregularly. Such discrepancies between the amount of insulin administered and IOB can cause dramatic fluctuations in glucose levels, posing great risks to patients.[7] A direct method of monitoring insulin in circulation would allow real-time adjustments to IOB prior to glucose level deviations.

The addition of an insulin sensor can address the limitations of the current diabetes monitoring technology. In concert with the CGM, the insulin sensor notifies the artificial pancreas when to administer insulin. With this goal in mind, we are developing a FRET optical biosensor to continuously monitor insulin. The native insulin receptor (InR) provides the starting point for our project's "optimization through mutagenesis" approach. The InR has reversible binding with fast kinetics and produces a conformational change that can be observed by FRET.[8] With directed evolution via phage display, we aim to develop and recombinantly express an InR variant that binds to insulin to assess binding kinetics, limit of detection, and dynamic range of sensing at physiological concentrations.

Project II: Real-time calcium sensing for clinical applications

For sensor development, we explored a calcium sensing model system. A fluorophore-linked calcium sensing protein, of a similar size to the InR variant, was designed to assess the FRET-ability of the construct. Additionally, this calcium sensing project could open opportunities to address new applications in physiology and treatment.[9] Calcium level monitoring could improve activity assessments for applications in sports medicine and physical therapy. In addition, it can provide vital signs during organ transplantation or exchange transfusion, and managing calcium-related diseases, such as kidney dysfunction, hyperparathyroidism, and osteoporosis.[10]

Currently, endogenous calcium can be quantified by Abbott's i-STAT® point-of-care device. The i-STAT® measures analytes in the patient's blood and produces results within two minutes.[9,11] Although the device provides rapid and lab-quality results, the required blood sample limits real-time measurements and its use for neonatal and elderly patients.[9,11] In addition to i-STAT, continuous calcium sensors have been fabricated through the functionalization of calcium-specific ionophores on nanorods and calcium sensing proteins.[12,13] These studies were unable to demonstrate reversible calcium binding dynamics, dose-dependent response, or implantability of the device.[12,13] To address these limitations, we are developing a biosensor to continuously monitor the dynamics of calcium concentration by FRET.

Genetically encoded calcium indicators use FRET to quantify intracellular calcium by taking advantage of the conformational change in a calcium sensing protein, calmodulin, upon binding.[14,15,16] In recent studies, troponin C, a calcium binding protein responsible for muscle contraction, shows reversible binding kinetics, stability *in vivo,* and sensitivity to calcium concentrations, making it an excellent candidate for this project.[16] A troponin C construct, Twitch-2B, showed the most promising results in that it is smaller, displays high FRET changes, and is brighter than other constructs when using cpVenus^{CD} and mCerulean3 FRET pair.[16,17] For the

calcium sensor, we expressed a recombinant form of Twitch-2B with chemically linked protein fluorophores and analyze the FRET of Twitch-2B to incorporation into an optical biosensor.

RESULTS AND DISCUSSION

Project I: Real-time insulin sensor for T1D management

1.1 Rationale for the usage of InR C4

My colleague, Sanjana Sen, designed six InR constructs based on the wild-type protein (Figure 1A). The wild-type InR consists of a transmembrane domain and an extracellular domain, which binds to insulin. The extracellular domain consists of a disordered region at the N-terminus (Pre), two leucine-rich repeat domains (L1 and L2), a cysteine-rich domain (CR), two fibronectin type-III domains (FnIII 1 and FnIII 2α), an insert domain (IDα), and a chain of carboxyl terminal (αCT).[18,19] The wild-type InR has two binding sites for insulin; the L1 domain curves towards αCT to form the high affinity binding site 1, and the FnIII 1 domain forms the low affinity binding site 2 (Figure 1B).[20,21,22] Our investigation focuses on construct 4 (InR C4), as it is the most soluble following *Escherichia coli (E.coli)* expression. The domain is also the smallest of the constructs and can be displayed on M13 phage surface (data not shown) for future evolution and engineering.

Figure 1. (**A**) Schematic of the wild-type InR and its six constructs. The construction of a mutagenesis library uses InR C4, highlighted in green, as a template for directed evolution via phage display. (**B**) Protein structure of the wild-type InR with the insulin binding regions shown in shades of blue. Insulin is shown in pink (PDB entry

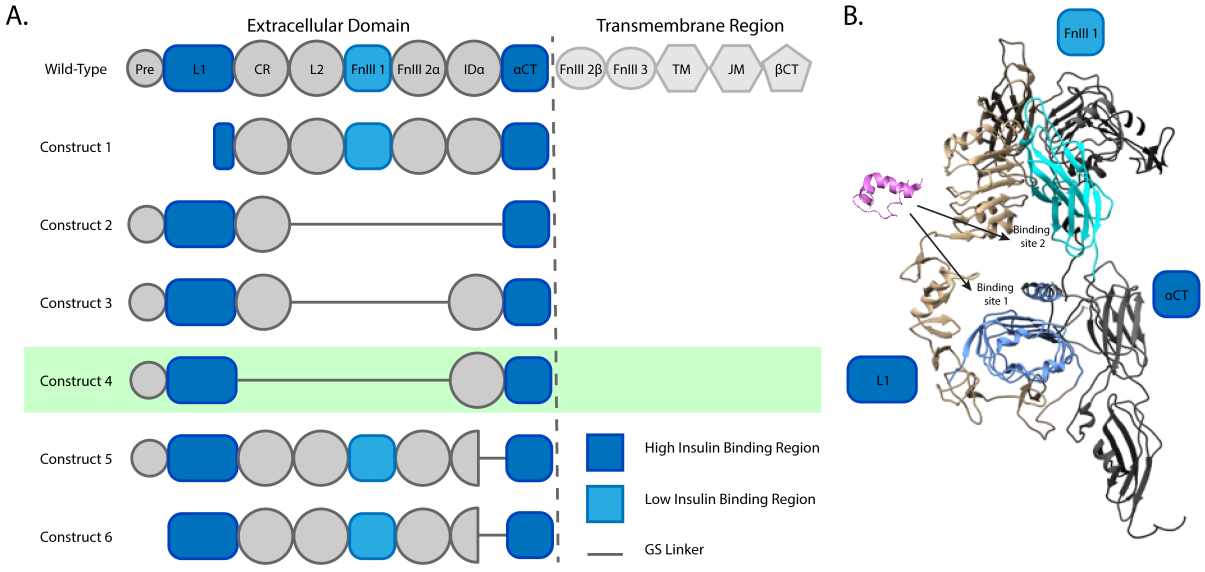

1.2 Construction of the error prone InR C4 library into ER2738 phage display cells

In the dimer form, InR oligomerizes, via disulfide bridges, to form a large complex. A small protein is beneficial for biosensing purposes as it can allow ease of modification and immobilization onto the sensor in a predefined orientation.[23] To preferentially purify the monomer, the disulfide bonds were eliminated between the InR dimers by substituting out the three disulfide-forming cysteine residue with serines and alanines as follows: C241S, C242A, and C244S (Table S1, S2).

Using random mutagenesis, we aim to scour the gene sequence for mutational hot spots (regions with clustered mutations). This systematic approach allows insight into areas responsible for increased insulin binding affinity and focused site-saturation mutagenesis. To achieve this goal, error-prone PCR (epPCR) was used to generate random mutations throughput the length of the

InR C4 construct. The error-prone library was then subcloned into an M-13 bacteriophage vector plasmid, phagemid (Table S2 and Figure S1A). Several epPCR conditions and ligation methods were tested towards preparing the library (e.g. ligation independent cloning and Golden Gate Assembly), but efficiency was low. Gibson assembly, however, yielded successful cloning of the InR C4 error-prone library into the phagemid with greater efficiency.

With a prepared library, cellular uptake into phage display electrocompetent cells via electroporation was required for directed evolution of the InR C4. The use of *Rec* A-ER2738 phage display electrocompetent cells replaced SS320 cells to reduce gene recombination and InR gene fragmentation that was previously observed (Figure S1B). Electroporation of the ER2738 cells generated high titers, 10^8 colony forming units (cfu) of cells and 10^7 cfu of library-containing cells (Figure S1C).

1.3 Identification of high-affinity insulin binders within the library

From the epPCR library, we aimed to identify InR variants that bound insulin greater than three-fold over the background protein, bovine serum albumin (BSA). Briefly, monomeric insulin was covalently conjugated to magnetic beads and used to select phage displayed InR C4 library variants that bind insulin (Figure S2A). Three systematic rounds of phage display selections were designed (Table 1). Selections using anti-FLAG isolated only full-length constructs. These selectants were used to bind insulin for two rounds with increased stringency (washes) and varied blocking reagents to ensure that selectants specifically bound insulin and not the blocking buffer. In each round of selections, the ER2738 cells maintained high diversity (Figure S2B).

Table 1. Details of the selection process and the resulting titers for the InR C4 phage library.

Round	*Target*	*Blocking*	*Washes*	*Cell Titers (cfu)*	*Library Cell Titers (cfu)*
1	Anti-FLAG	BSA	6	10^{10}	10^{8}
2	Insulin	Casein	6	10^{10}	10^{7}
3	Insulin	HSA	9	10^{9}	10^{9}

After selections, 96 colonies of selectants were individually grown and screened by a phage-based enzyme-linked immunosorbent assay (ELISA) to screen for high-affinity insulin binders. In one approach, the wells were coated with the monomeric insulin, blocked with BSA, and incubated with the individual selectants. Finally, a horseradish peroxidase (HRP)-conjugated phage-specific antibody was used to detect phage with affinity for insulin (Figure 2A). This ELISA format did not identify any insulin binders. It was hypothesized that the absence of InR variant biding to insulin on the ELISA plate was due to the insulin being coated on the plate surface and most of its surface being inaccessible. In an alternative format, the wells were coated with an anti-M13 antibody, that targets the bacteriophage's P8 protein, blocked with BSA, incubated with the individual selectants, and exposed to biotinylated insulin in solution. A streptavidin-HRP conjugate was used to detect binding colorimetrically (Figure 2B, S2C-D). With this method, nine phage selectants were identified as potential high-affinity binders (Figure 2C). DNA sequences for these mutations were then determined using Sanger sequencing.

Of the nine identified binders, only phage selectant 52 contained a full-length InR C4 DNA sequence. Due to low-quality sequencing results, selectant 52 was deconvoluted by retransforming and isolating the plasmids of five random colonies. Interestingly, sequencing of these colonies identified two distinct mutational patterns. Colonies 52-1, 52-3, and 52-4 contained a STOP codon (TGA) at position 181, which would prevent display on the phage surface whereas colonies 52-2

and 52-5 showed a second set of entirely different mutations (Figure 2D), a complete sequence without STOP codons and with 9-10 mutations. It was concluded that the full-length sequence (52-2) was responsible for insulin binding. Therefore, the full-length variant 52-2 was subcloned into a pRSET vector, containing a cyan fluorescent protein (CFP) and a yellow fluorescent protein (YFP) flanking the N- and C- terminus, respectively, to generate an InR FRET construct.

Figure 2. (**A**) A schematic for an ELISA assay with an insulin-coated plate. (**B**) Schematic for a phage-coated assay. (**C**) Results from screening phage-display InR C4 library selectants for insulin binding. Colonies that bind insulin > 2.5x over background (BSA) are considered "hits". Colony 52 and 94 are highlighted here. (**D**) A 96-well ELISA screening with phage-coated plates displaying the corresponding color change for each selectant screened. Selectant 52 resulted in a full-length sequence and displayed two distinct mutational patterns. (**E**) Colony 52-2 FRET response to Humalog®.

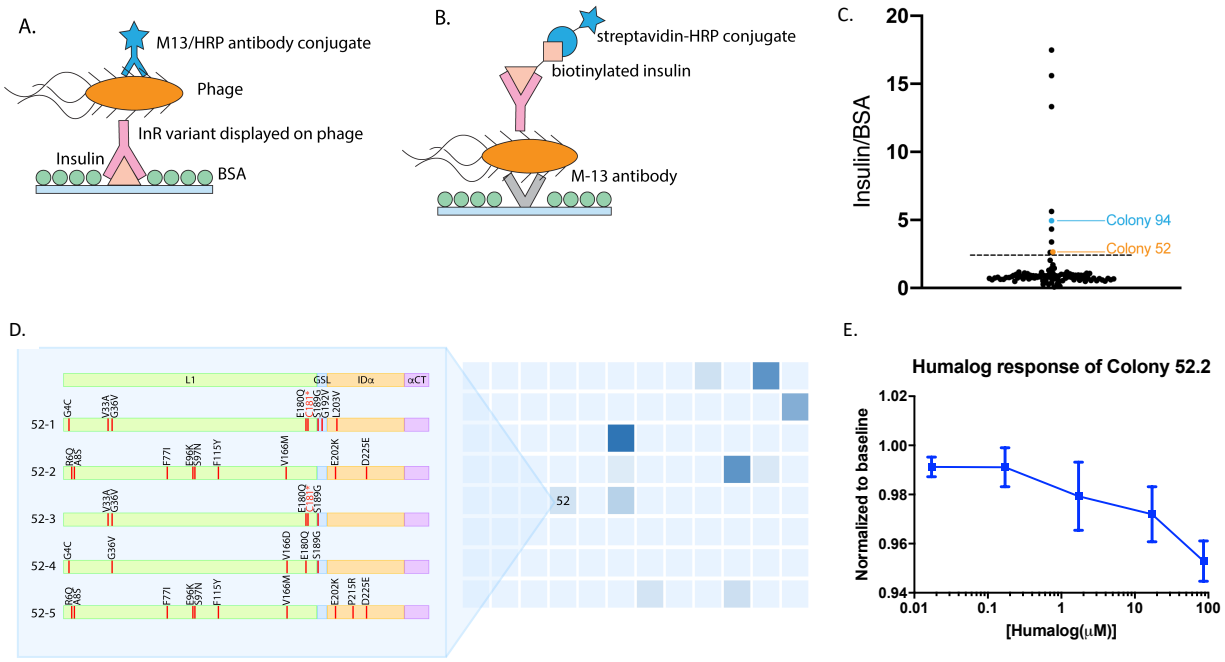

The FRET construct for colony 52-2 was expressed in *E. coli* in BL21DE3 cell lines. We developed a mid-throughput screening assay for testing dose-dependent FRET. The assay was developed using the insulin analog, Humalog® (Eli Lilly). Humalog® is a commonly used form of insulin in T1D patients for real-time management of glucose and can be stored long-term without aggregating. The results show large errors bars in the response of the peptide to varying

concentrations of Humalog®, but there is a difference between the lowest and highest concentrations tested (Figure 2E).

1.4 Rationale for the creation of InR C7

From the phage display library of InR C4, the fragmented hits were further analyzed. Of these, only colony 94 maintained the αCT, a high affinity insulin binding region (Figure 2C). From her work with another InR construct, Sanjana Sen had found that constructs that are less than 30 amino acids show strong baseline FRET signals because of the close proximity of the FRET pair fluorophores. Because of the flexibility of the unstructured Idα, the distance in Angstroms between the fluorophores is unknown. Therefore, it is challenging to observe changes in FRET for different concentrations of insulin with appropriate signal-to-noise for short constructs with <30 amino acids. Because colony 94 has 54 amino acids and maintains the αCT, InR C7 was created for library production and analysis (Figure 3A).

The partial IDα and the complete αCT binding domain in colony 94 was cloned into the pRSET vector flanked with genetically encoded CFP and YFP at the N- and C-termini, respectively. This new InR FRET construct, InR C7, was solubly expressed in BL21DE3 cell lines and purified using Nickel-nitrilotriacetic acid (Ni-NTA) His-tag affinity purification (Figure S3A-B). To determine whether the C-terminal binding domain of the InR was sufficient to bind insulin specifically, the purified InR C7 was tested for binding to insulin and its homolog, IGF-I, via ELISA. Results demonstrated that InR C7 bound insulin with greater affinity than IGF-I (Figure 3B).

After establishing that InR C7 bound insulin with some specificity, we examined whether this binding would translate to conformational change and FRET signal. Purified InR C7 was

tested for a change in FRET signal in response to varying doses of Humalog® from 170 pM to 6 µM. The results did not show any change in FRET signal of InR C7 upon treatment with Humalog® relative to baseline controls. The same FRET analysis was conducted with unpurified InR C7 lysate. This experiment was performed by undergraduate student Keertna Bhuvan, who then tested InR C7 lysate with varying doses of Humalog®. In this experiment, InR C7 demonstrated increase dose-dependent FRET in response to Humalog®. We observed that there is a dose-dependent response between the clinically relevant concentrations of insulin (12 pM – 2nM), although small (Figure 3C).

Figure 3. (**A**) Schematic of the wild-type InR protein, InR C4, and InR C7. (**B**) A schematic of the specificity ELISA performed. InR C7 showed greater affinity to insulin compared to IGF-I and the background (casein). (**C**) Schematic of the 96 well FRET assay method from plasmid transformation, to cell growth and protein production in 96-deep-well plates and assay preparation. FRET response is displayed as acceptor peak values at 525 nm normalized to donor peak (475 nm). The graph shows dose-dependent response of InR C7 to Humalog® within physiological range (yellow box).

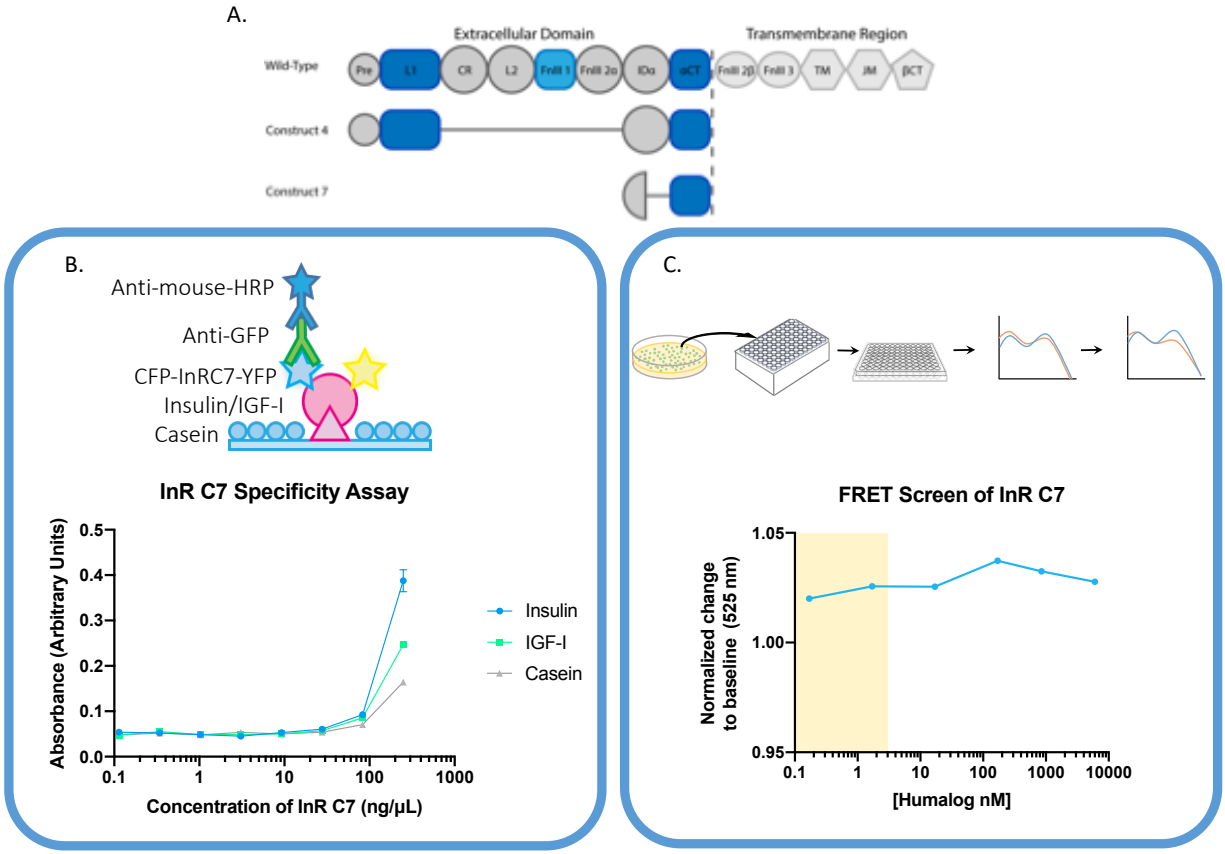

1.5 Construction of the error prone InR C7 library in E. coli

While InR C7 had shown preferential binding to insulin, the magnitude of the FRET response to varying doses of Humalog® was very small and not consistently dose-dependent. A library of InR variants using InR C7 as a template was created via random mutagenesis by error-prone PCR. The library was transformed into BLR (DE3) cell line. To verify the quality of the library, random colonies were chosen for Sanger sequencing to determine what percentage of the variant population contained random mutations (threshold >60%). Sequencing results demonstrated a mutagenesis efficiency of 67% (4 out of 6), which was considered suitable for further screening.

The library was prepared for FRET analysis (Figure 3C). Several screened colonies demonstrated changes in FRET in response to varying doses (0.01 - 100 nM) of Humalog®. Potential hits were selected based on changes in FRET responses above the largest standard deviation (σ) among all the dose responses to Humalog® by the wild-type InR C7 measured in triplicate (Figure 4A). Ten potential hits were sequenced using Sanger sequencing. Unfortunately, we observed that many of the potential hits had the sequence of wild-type InR C7 indicating that the InR C7 response may be inconsistent based on factors that are uncontrolled by the current mid-throughput assay, such as exact optical density at induction, protein concentration, and growth effects based on plate position (Figure 4B). Two variants did demonstrate mutations very close in proximity in the amino acid sequence. While these variants are within the noise of the other wild-type InR C7 variant, they will be further investigated to determine whether they generate a more consistent response to Humalog® than the wild-type InR C7.

Figure 4. (**A**) Dose-dependent response to Humalog® where the yellow box highlights the concentration of insulin at physiological range. **(B)** Table of randomly sequenced colonies to determine the efficiency of the epPCR used to generate the random mutagenesis InR C7 library. The majority of the potential hits had the sequence of wild-type InR C7, while two exhibited mutations.

A.

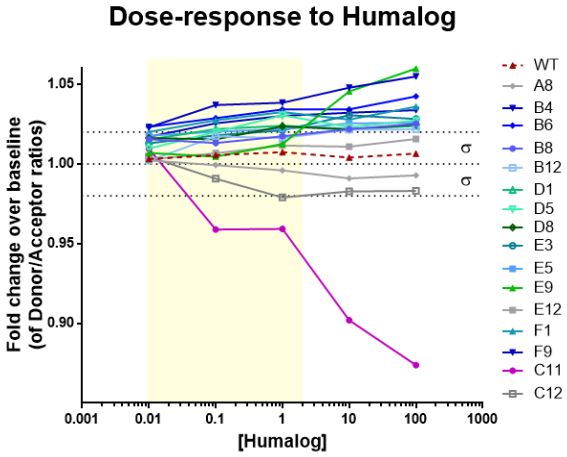

B.

Colony Name	Mutations
B4	WT
B6	WT
B8	P345S
B12	E326G
D1	WT
D8	WT
E3	WT
E5	WT
F1	WT
F9	WT

1.6 Exploration in construct InR Pep6C7

Sanjana Sen previously worked on a Mega Random Peptide Library (MRPL) in 2017 where she investigated six peptides from the library for their specificity to various substrates, including insulin and IGF-I. Peptide 6 demonstrated specificity for insulin over IGF-I (Figure 5A). This peptide is 20 amino acids long, which is too short for FRET analysis. We rationalized a new construct that fuses peptide 6 to InR C7 to increase conformational change upon binding Humalog® and increase the specificity for Humalog® over IGF-I. This new construct was called InR Pep6C7 (Figure 5B).

When Pep6 was explored by Sanjana, it bound to insulin in an unknown direction. When tethered to InR C7, the direction of Pep6 is important to ensure proper binding. Therefore, two sub constructs were created, in which Pep6 is tethered to InR C7 in either an arbitrary forward or reverse direction (InR Pep6C7 F and InR Pep6C7 R). CFP-InR Pep6C7 F-YFP and CFP-InR Pep6C7 R-YFP were cloned using the existing pRSET CFP-InR C7-YFP plasmid. Both variant

proteins were expressed following similar conditions to InR C7 expression (Figure S4). Initially, these expression conditions resulted in an impure sample. SDS-PAGE analysis after purification suggested that the protein may have degraded during the expression. Altering expression conditions with a shorter induction time improved the protein yield and purity (Figure S4).

An insulin and IGF-I ELISA binding assay was conducted to determine whether InR Pep6C7 F or R proteins could specifically bind insulin (Figure 5C-D). InR Pep6C7 F showed preferential binding to insulin over IGF-I, and InR Pep6C7 R did not. InR Pep6C7 F and R were then analyzed for FRET in the presence of varying Humalog® concentrations using a fluorescence plate reader. Unfortunately, ELISA binding results conflicted with the FRET assay, where InR Pep6C7 F did not show a dose-dependent response to insulin, but InR Pep6C7 R did. Because of these conflicting data, we focused our efforts on InR C7.

Figure 5. (A) Specificity assay of peptide 6 from the MRPL library. **(B)** Schematic of the wild-type InR, InR C4, InR C7, and InR Pep6C7. (**C**) Specificity assay of InR Pep6C7 F. **(D)** Specificity assay of InR Pep6C7 R.

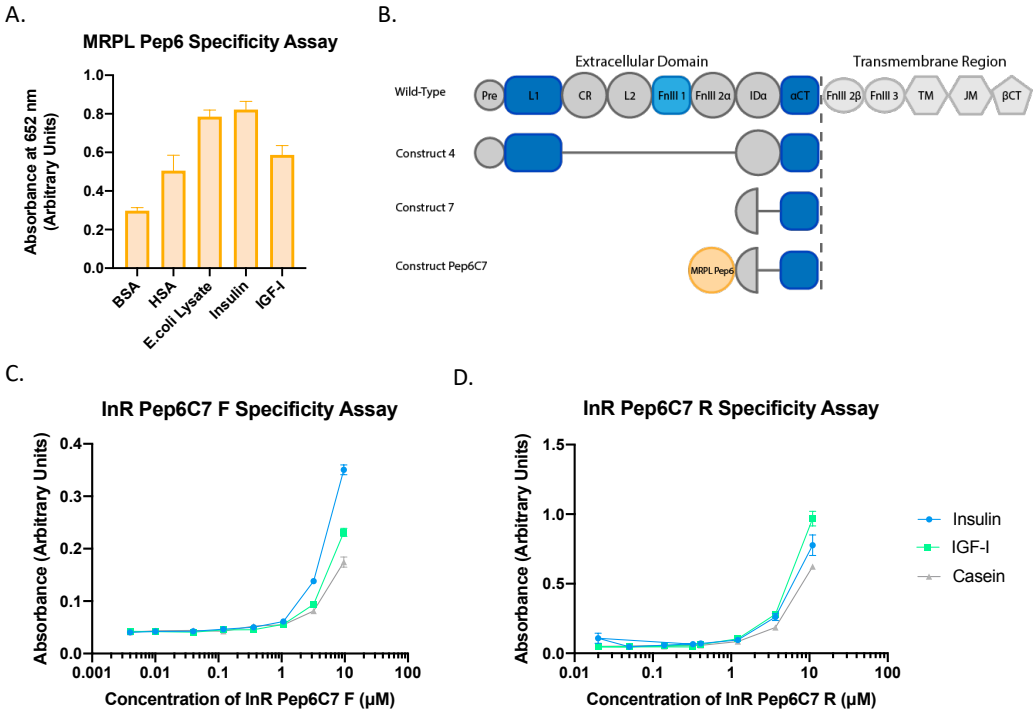

1.7 Exploration in an IDDel construct

In order to increase the likelihood that FRET might occur upon binding, the distance between the two high affinity binding domains, L1 and αCT were shortened by a partial deletion of the flexible IDα. Sanjana Sen and Keertna Bhuvan rationally designed this new construct known as IDDel (Figure 6A). Sanjana Sen and Keertna Bhuvan expressed the protein for CFP-IDDel-YFP and conducted preliminary tests. Results demonstrated that InR C4 and IDDel demonstrated no change in FRET signal in response to varying dose of insulin (Figure 6B). In order to improve folding of the IDDel construct, an error-prone library of IDDel was created. The IDDel protein was difficult to express and analyze for FRET. Conditions with glucose and PEG were tested to optimize the expression and FRET analysis, respectively (Figure 6C).

Sanjana Sen, Keertna Bhuvan, and I worked together to screen the fluorescence of approximately 600 variants of the library by varying Humalog® concentrations and monitoring FRET response with a fluorescence plate reader (Figure 6D). Many of the sequences that demonstrated a FRET response at baseline and further FRET increases with insulin very highly fragmented and were likely responding to a change in overall crowding in solution. Two full-length sequences demonstrated a slight dose-dependence in response to Humalog®. Interestingly, two out of three of the mutations from these hits are located on the binding interface of InR and insulin, in the L1 domain (Figure 6E). NDT libraries were generated of the three sites. However, no reliable response to Humalog® was observed. Hits that are observed in 96-well format are unable to be repeated due to plate position effects and differences in total protein concentrations. In order to reduce variability between wells, a 24-deep-well plate will be used to assay hits in triplicate.

Figure 6. (A) Schematic of the wild-type InR, InR C4, InR C7, and IDDel. **(B)** IDDel gives a FRET response to Humalog®. (**C**) Glucose and PEG conditions were tested to optimize the protein expression. (**D**) Several dose-dependent hits were obtained from the error-prone IDDel library. (**E**) Table of mutations for the dose-dependent hits in 6D. *R1L4S3 B1* did not display any mutations because it was extremely truncated.

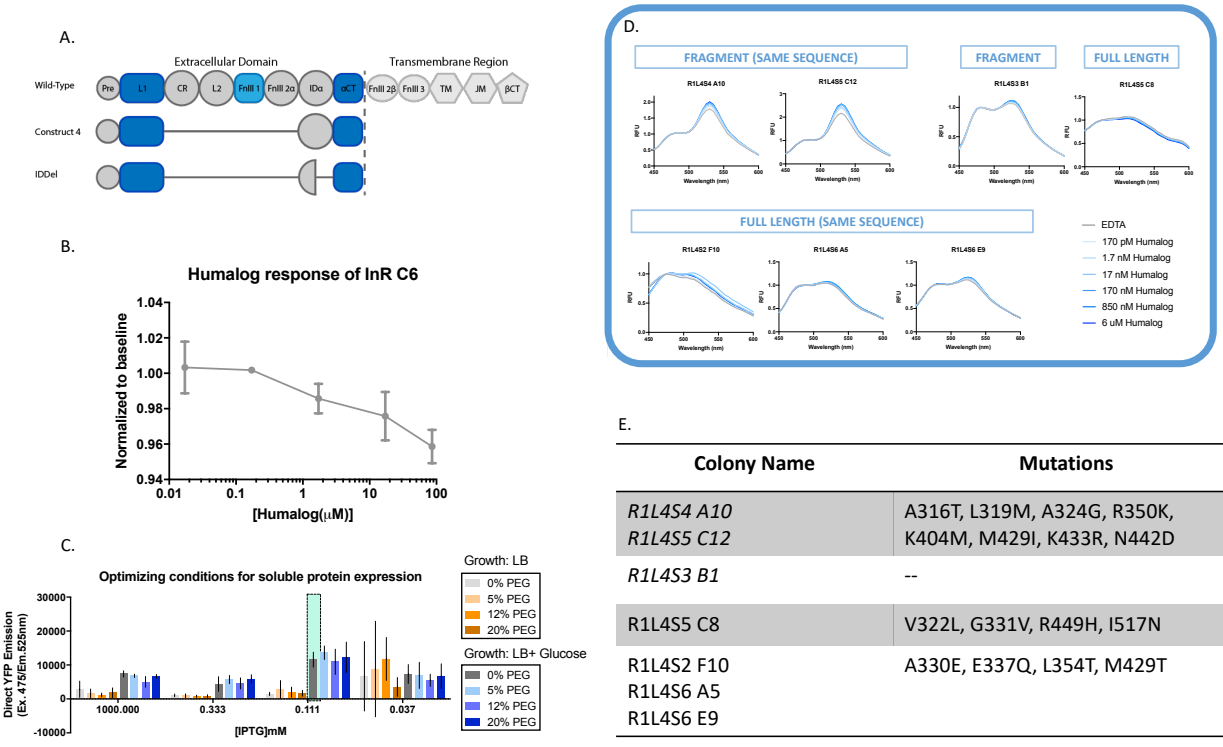

E.

Colony Name	Mutations
R1L4S4 A10 *R1L4S5 C12*	A316T, L319M, A324G, R350K, K404M, M429I, K433R, N442D
R1L4S3 B1	--
R1L4S5 C8	V322L, G331V, R449H, I517N
R1L4S2 F10 R1L4S6 A5 R1L4S6 E9	A330E, E337Q, L354T, M429T

Project II: Real-time calcium sensing for clinical applications

2.1 FRET studies on Twitch-2B fused between CFP and YFP

To build a calcium sensor, I cloned and expressed a fusion protein of CFP, YFP, and Twitch-2B (CFP-Twitch-2B-YFP) (Table S3 and Figure S5A). Former Weiss Lab member, Dr. Gaetano Speciale, optimized the expression and purification of the protein (Figure S5B). In the case where the Twitch-2B protein was encapsulated in an optical fiber.

Figure 7. YFP fluorescence decreases over the span of one hour, showing signs of photobleaching.

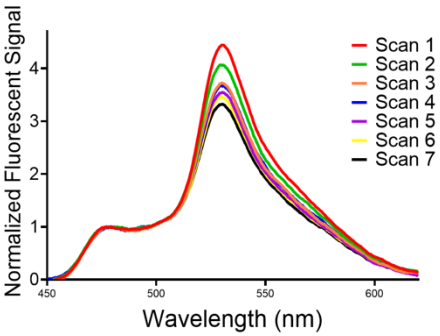

Incubated in 3-morpholinopropane-1-sulfonic acid (MOPS) buffer with fluorescence readings measured in ten-minute intervals (Figure 7) it was observed that the FRET signal decreased due to loss of overall YFP fluorescence. The conditions of the experiment within the optic fiber device permanently damaged the YFP from prolonged light exposure, a phenomenon known as photobleaching.[24] To develop a sensor for long-term use in patients, it was necessary to move away from genetically-encoded fluorophores that are prone to photobleaching and investigate means of the bioconjugation of stable, and high quantum yield small molecule FRET pairs.

2.2 Expression and purification of SNAP-Twitch-2B-CLIP for FRET analysis

To minimize photobleaching, we replaced the recombinant fluorophores with SNAP- and CLIP-tags (Table S3) for post-translational modification with fluorophores (Figure 8A). These recombinant fusion proteins are similar in size (19 kDa) and structure for ease of optimization of expression. The CLIP-tag and the SNAP-tag originate from a DNA repair protein found in humans, O^6-alkylguanine-DNA alkyltransferase.[25] Fluorophores containing O^6-benzylguanine (BG) or O^2-benzylcytosine (BC) chemical moieties can orthogonally and covalently bind the SNAP- and CLIP-tag, respectively.[25]

We chose to label the SNAP- and CLIP-tag with BG-Alexa Fluor 488 and BC-Alexa Fluor 546, respectively. This well-established FRET pair is more photostable than CFP and YFP. Additionally, BC-Alexa Fluor 546, is also more pH stable than YFP. Most importantly, the fluorophores can easily be conjugated to SNAP-Twitch-2B-CLIP in a one-pot reaction. Thus, a fused SNAP-Twitch-2B-CLIP protein bioconjugated to BG and BC fluorescent probes will serve as a new detection platform for the calcium sensor.

To express and purify SNAP-Twitch-2B-CLIP, the protein expression protocol for CFP-Twitch-2B-YFP was troubleshot and optimized. Initial expressions were plagued by low yield and loss of protein through precipitation. To accommodate the stability and functionality of the new construct, the expression was scaled up by four to produce a sufficient amount of protein and long-term storage was explored (Figure S6). To address stability, I experimented with three different buffers: (1) 50 mM Tris-HCl, 300 mM NaCl, pH 7.4; (2) 50 mM Na_3PO_4, 300 mM NaCl, pH 7.4; (3) 50 mM HEPES, pH 7.4.[13] After a week, the samples showed no evidence of precipitation. Future expressions were carried out in HEPES buffer due to the pH stability of the buffer.

Figure 8. (**A**) A schematic of SNAP-Twitch-2B-CLIP undergoing site-specific tagging with the fluorophores and producing different signals in the absence and presence of calcium. (**B**) SDS-PAGE gel of SNAP-Twitch-2B-CLIP after purification. (**C**) Combined fluorescence gel of the site-specific tagging of the fluorophores in triplicate (left), fluorescence gel of BG-Alexa Fluor 488 (top right), and fluorescence gel of BC-Alexa Fluor 546 (bottom right). (**D**) Fluorescence graph of SNAP-Twitch-2B-CLIP with calcium and EGTA.

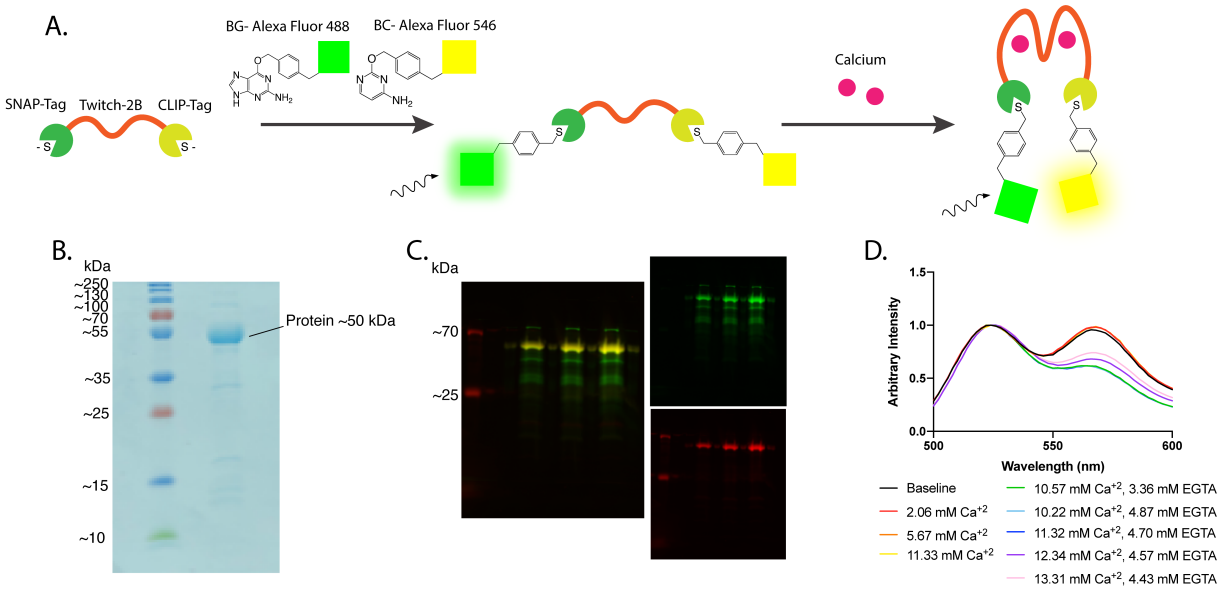

Before covalently linking the protein to BG-Alexa Fluor 488 and BC-Alexa Fluor 546, an additional purification step was required to reduce off-target bioconjugation or any hindrance in reaction efficiency. The protein was purified by fast protein liquid chromatography system (FPLC)

on a Superdex75 10/300 analytical column (Figure 8B). After fluorophore tagging, further purification was performed to remove unbound fluorophores. The fluorescence gel shows specific tagging of SNAP and CLIP with their respective fluorophores in triplicate with increasing protein volume (Figure 8C). Although BC-Alexa Fluor 546 was highly specific, BG-Alexa Fluor 488 also modified residual lysate.

With the tagged SNAP-Twitch-2B-CLIP, my collaborator from Dr. Elliot Botvinick's lab, Dat Nguyen, analyzed the protein's ability to FRET in response calcium. The expected FRET results were observed in response to varying doses of calcium and ethylene glycol-bis(β-aminoethyl ether)-*N,N,N',N'*-tetraacetic acid (EGTA), a calcium chelator (Figure 8D). This FRET experiment further validated the site-specific tagging of SNAP- and CLIP-tags and demonstrate that replacing genetically encoded fluorophores with the SNAP-CLIP system did not impact the function of Twtich-2B as a calcium FRET sensor. We further demonstrated that the new SNAP-Twitch-2B-CLIP FRET construct overcomes the photobleaching challenge, thereby making sensor testing within the optical fiber device feasible. Furthermore, tests conducted by Dat Nguyen on the optical fiber sensor demonstrated that the device protects the SNAP-Twitch-2B-CLIP construct from proteinase K degradation and allows stable uninterrupted calcium sensing.[26]

CONCLUSION AND FUTURE WORKS

For projects I and II, phage and *E. coli* libraries were constructed and the photostable version of the Twitch-2B calcium sensor, SNAP-Twitch-2B-CLIP, was developed. For Project I, InR C4 variants were tested and identified nine selectants with increased binding to insulin. Of the nine selectants, one exhibited a mutational pattern that was hypothesized to be responsible for

insulin binding. In addition, further constructs were explored and aided in assay development. For Project II, conditions were varied to express and purify SNAP-Twitch-2B-CLIP that replaced CFP-Twitch-2B-YFP. The new FRET construct overcame a serious issue of photobleaching, making the project feasible for its application. It was speculated the site-specific tagging of the SNAP- and CLIP-tags with Alexa Fluor dyes and its ability for FRET. The resulting protein construct is a candidate for a continuous calcium sensor.

Future work with the biomedical engineering collaborators will focus on building a FRET sensor for T1D. A continuation of high throughput screens for a FRET response to insulin will aid in determining essential mutations for staggered extension PCR libraries, followed by iterative site-saturation mutagenesis.[27] To create a more effective InR variant, additional screenings for the selectivity of insulin over insulin-like growth factor-I, variants that are more responsive to insulin over IGF-I will be sorted. In addition, an IGF-I sensor can be built using the hits that were selective for IGF-I as its basis.

The described work will help build a continuous optical FRET sensor that can apply towards effective monitoring, diagnostic, and therapeutic purposes. To make the devices practical for health applications, we need thorough *in vitro* and *in vivo* studies at the forefront of protein engineering and device manufacturing. This will overcome scientific challenges that often occurs when one is unaware of the limitations of the other.[28] In addition, we need to consider regulatory, ethical, and legal challenges as the device progresses.[28] Doing so will ensure the improvement of the artificial pancreas and safety of the patients.

REFERENCES

1. Turner, A. P. F. Biosensors: Sense and Sensibility. *Chem. Soc. Rev.* 2013, *42*, 3184–3196.
2. Damborský, P.; Švitel, J.; Katrlík, J. Optical Biosensors. *Essays Biochem.* 2016, *60*, 91–100.
3. Bajar, B. T.; Wang, E. S.; Zhang, S.; Lin, M. Z.; Chu, J. A Guide to Fluorescent Protein FRET Pairs. *Sensors* 2016, *16*, 1–24.
4. Centers for Disease Control and Prevention. https://www.cdc.gov/diabetes/pdfs/data/statistics/national-diabetes-statistics-report.pdf (accessed August 24, 2019).
5. *Hyperglycemia and hypoglycemia in type 1 diabetes.* Institute for Quality and Efficiency in Health Care (IQWiG): Cologne, Germany; 2007.
6. Herman, A.; Montjoye, L.; Tromme, I.; Goossens, A.; Baeck, M. Contact Dermatitis, 2018, *79*, 331-335.
7. Ellingsen, C.; Dassau, E.; Zisser, H.; Grosman, B.; Percival, M. W.; Jovanovič, L.; Doyle, F. J. Safety Constraints in an Artificial Pancreatic β Cell: An Implementation of Model Predictive Control with Insulin on Board. *J. Diabetes Sci. Technol.* 2009, *3* (3), 536–544.
8. Lee, J.; Pilch, P. F. The Insulin Receptor: Structure, Function, and Signaling. *Am. J. Physiol*. 1994, 319-334.
9. Seshadri, D. R.; Li, R. T.; Voos, J. E.; Rowbottom, J. R.; Alfes, C. M.; Zorman, C. A.; Drummond, C. K. Wearable Sensors for Monitoring the Physiological and Biochemical Profile of the Athlete. *npj Digital Medicine*, 2019, *2.*
10. Yuen, N. K.; Ananthakrishnan, S.; Campbell, M. J. Hyperparathyroidism of Renal Disease. *Perm. J.* 2016, *20*, 78–83.
11. Bandodkar, A. J.; Wang, J. Non-Invasive Wearable Electrochemical Sensors: A Review. *Trends Biotechnol.* 2014, *32*, 363–371.
12. Asif, M. H.; Fulati, A.; Nur, O.; Willander, M.; Brännmark, C.; Stråfors, P.; Börjesson, S. I.; Elinder, F. Functionalized Zinc Oxide Nanorod with Ionophore-Membrane Coating as an Intracellular Ca2+ Selective Sensor. *Applied Physics Letters*, 2009, *95,* p. 023703.
13. Hall, W. P., Anker, J. N., Lin, Y., Modica, J., Mrksich, M, Van Duyne, R. P.; A Calcium-Modulated Plasmonic Switch. *J. Am. Chem. Soc.*, 2008, *130*, 5836–5837.
14. Ishitsuka, Y.; Azadfar, N.; Kobitski, A. Y.; Nienhaus, K.; Johnsson, N.; Nienhaus, G. U. *J. Phys. Chem. B.* 2015, *119*, 6611–6619.
15. Guo, Z.; Johnston, W. A.; Whitfield, J.; Walden, P.; Cui, Z.; Wijker, E.; Edwardraja, S.; Retamal Lantadilla, I.; Ely, F.; Vickers, C.; Ungerer, J. P. J.; Alexandrov. K. Generalizable Protein Biosensors Based on Synthetic Switch Modules. *J. Am. Chem. Soc*. 2019.
16. Thestrup, T.; Litzlbauer, J.; Bartholomäus, I.; Mues, M.; Russo, L.; Dana, H.; Kovalchuk, Y.; Liang, Y.; Kalamakis, G.; Laukat, Y.; Becker, S.; Witte, G.; Geiger, A.; Allen, T.; Rome, L. C.; Chen, T.; Kim, D. S.; Garaschuk, O, Griesinger, C.; Griesbeck, O. Optimized Ratiometric Calcium Sensors for Functional in Vivo Imaging of Neurons and T Lymphocytes. *Nat. Methods* 2014, *11*, 175–182.
17. Trigo-Mourino, P.; Thestrup, T.; Griesbeck, O.; Griesinger, C.; Becker, S. Dynamic Tuning of FRET in a Green Fluorescent Protein Biosensor. *Sci. Adv.* 2019, *5*, eaaw4988.
18. De Meyts, P. *The Insulin Receptor and Its Signal Transduction Network.* Feingold KR, Anawalt B, Boyce A, Chrousos G, Dungan K, Grossman A, Hershman JM, Kaltsas G, Koch C, Kopp P, Korbonits M, McLachlan R, Morley JE, New M, Perreault L, Purnell J, Rebar R, Singer F, Trence DL, Vinik A, Wilson DP, Ed.; MDText.com, Inc.: South Dartmouth; 2016.

19. Dehghan-Shasaltaneh, M.; Lanjanian, H.; Riazi, G. H.; Masoudi-Nejad, A. The Importance of α-CT and Salt Bridges in the Formation of Insulin and Its Receptor Complex by Computational Simulation. *Iran. J. Pharm. Res.* 2018, *17*, 63–74.
20. Croll, T. I.; Smith, B. J.; Margetts, M. B.; Whittaker, J.; Weiss, M. A.; Ward, C. W.; Lawrence, M. C. Higher-Resolution Structure of the Human Insulin Receptor Ectodomain: Multi-Modal Inclusion of the Insert Domain. *Structure* 2016, *24* (3), 469–476.
21. McKern, N. M.; Lawrence, M. C.; Streltsov, V. A.; Lou, M. Z.; Adams, T. E.; Lovrecz, G. O.; Elleman, T. C.; Richards, K. M.; Bentley, J. D.; Pilling, P. A.; Hoyne, P. A.; Cartledge, K. A.; Pham, T. M.; Lewis, J. L.; Sankovich, S. E.; Stoichevska, V.; Da Silva, E.; Robinson, C. P.; Frenkel, M. J.; Sparrow, L. G.; Fernley, R. T.; Epa, V. C.; Ward. C. W. Structure of the Insulin Receptor Ectodomain Reveals a Folded-over Conformation. *Nature* 2006, *443* (7108), 218–221.
22. Menting, J. G.; Whittaker, J.; Margetts, M. B.; Whittaker, L. J.; Kong, G. K. W.; Smith, B. J.; Watson, C. J.; Žáková, L.; Kletvíková, E.; Jiráček, J.; et al. How Insulin Engages Its Primary Binding Site on the Insulin Receptor. *Nature* 2013, *493* (7431), 241–245.
23. Barbosa, A. J. M.; Oliveira, A. R.; Roque, A. C. A. Protein- and Peptide-Based Biosensors in Artificial Olfaction. *Trends Biotechnol.* 2018, *36*, 1244–1258.
24. McAnaney, T. B.; Zeng, W.; Doe, C. F. E.; Bhanji, N.; Wakelin, S.; Pearson, D. S.; Abbyad, P.; Shi, X.; Boxer, S. G.; Bagshaw, C. R. Protonation, Photobleaching, and Photoactivation of Yellow Fluorescent Protein (YFP 10C): A Unifying Mechanism. *Biochemistry* 2005, *44*, 5510–5524.
25. Gautier, A.; Juillerat, A.; Heinis, C.; Corrêa, I. R.; Kindermann, M.; Beaufils, F.; Johnsson, K. An Engineered Protein Tag for Multiprotein Labeling in Living Cells. *Chem. Biol*. 2008, *15*, 128–136.
26. Nguyen, D.; Behrens, D. M.; Sen, S.; Najdahmadi, A.; Pham, J. N.; Speciale, G.; Lawrence, M. M.; Majumdar, S.; Weiss, G. A.; Botvinick, E. L. Photostable and Proteolysis-Resistant Förster Resonance Energy Transfer-Based Calcium Biosensor. *Anal. Chem.* 2020.
27. Zhao, H.; Zha, W. In Vitro "sexual" Evolution through the PCR-Based Staggered Extension Process (StEP). *Nat. Protoc.* 2006, *1*, 1865–1871.
28. Izmailova, E. S.; Wagner, J. A.; Perakslis, E. D. Wearable Devices in Clinical Trials: Hype and Hypothesis. *Clin. Pharmacol. Ther.* 2018, *104*, 42–52.